Structural Health Monitoring for Launch Vehicle Reusability Using Fiber Bragg Grating Written Optical Fibers

Thomas J. Colicci* and Andrew P. Noonan†
Vanderbilt University, Nashville, TN, USA

The reliance on Reusable Launch Vehicles (RLVs) is expected to increase as the space launch industry works towards reducing launch costs while focusing on sustainability. Monitoring the structural health of launch vehicle sections, especially those sustaining high dynamic loads and potential structural complications, is essential for re-flight certification. The objective of our current studies is to examine dynamic strain in rocket vehicle sections subjected to high loads during blast-charge-based separation events. In this context of Structural Health Monitoring (SHM) of launch vehicles, surface mounted Fiber Bragg Gratings (FBGs) offer distinct advantages over Resistive Strain Gauges (RSGs). The dynamic performance of FBG sensors and their comparison with RSGs is presented for dynamic impact studies on carbon fiber composite airframes using a calibrated impact test facility.

***This work is being done in collaboration with the Fiber Optic Strain Sensing Lab at NASA Armstrong Flight Research Center.**

I. Nomenclature

v	=	velocity
$t_{1\rightarrow2}$	=	time between sensor geometries 1 and 2
$t_{2\rightarrow3}$	=	time between sensor geometries 2 and 3
m	=	mass of drop plate
KE	=	kinetic energy
λ_B	=	Bragg Wavelength

II. Introduction

Carbon fiber composites are widely used in the design and manufacturing of Reusable Launch Vehicles (RLVs) and are favorable to traditional alloys on account of their strength-to-weight ratio and resistance to corrosion. These considerations make composites a leading candidate for material selection for pressure vessels and other load-bearing structures in flight. The demand for reusability necessitates Structural Health Monitoring (SHM) to accurately assess the condition of RLV components. The anisotropic nature of carbon fiber composites further demands experimental methods of evaluation.

Established methods of SHM such as laser Doppler vibrometry [1], Lamb wave detection [2, 3], and thermography [4] have been implemented in pre- and post-flight assessment in launch vehicle sections; this work seeks to implement a method of SHM that accounts for in-flight monitoring. The implementation of Fiber Bragg Grating (FBG) strain sensing provides many benefits in an in-flight monitoring use case, including insensitivity to electromagnetic interference, the ability to multiplex many sensors along a single fiber or sensor input channel, and a reduction in overall mass and physical profile compared to traditional in-flight systems [5]. The viability of adapting FBGs for an aerospace context has been extensively examined [6–11]. Additionally, studies involving the rate of strain application [2, 3, 12–14] and studies involving impact testing [15, 16] have been examined. This study examines the implementation of FBGs for the in-flight interrogation of dynamic strain.

*Graduate Student, Department of Mechanical Engineering, 2301 Vanderbilt Place, Nashville, TN, 37240, Student Member 1387437, Masters Category.

†Graduate Student, Department of Mechanical Engineering, 2301 Vanderbilt Place, Nashville, TN, 37240, Student Member 1373981, Masters Category.

The work presented investigates the performance of a collocated pair of FBG and RSG sensors on a carbon fiber airframe, subjected to point load impacts using a calibrated drop tower developed for the research. The drop tower ensures repeatable kinetic energy impact conditions that are comparable to high-strain rate events in flight. The next phase of this research will examine deployment events in Ground-Based Testing (GBT) in preparation for flight.

III. Facility Design

A. Dynamic Load Frame Design

A dynamic load frame was designed, built, and instrumented to monitor and characterize each impact. The drop tower is comprised of T-slotted aluminum, with an outer structural frame and an inner frame where the drop plate is connected. The drop plate moves along the T-slot using framing rollers. A 19 mm diameter round nose impact tup similar to those used in dynamic impact studies [15] was machined out of steel and mounted to the bottom of the drop plate to initiate the point load condition.

The initial condition of the drop is controlled using an electromagnetic end effector that holds the drop plate steady prior to an RF-controlled release. The height of the drop plate is controlled by a stepper motor assembly mounted to the top of the load frame that suspends the end effector by a pulley. A detailed schematic of the dynamic load frame testing architecture is provided below in Figure 2.

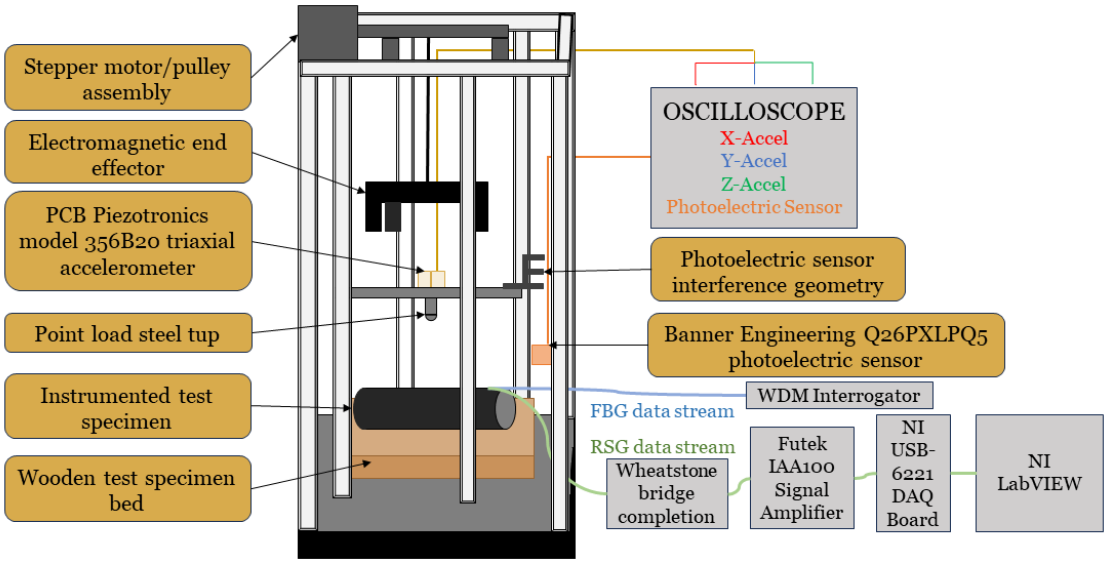

Fig. 1 Experimental overview of the dynamic load frame instrumentation and strain data streams.

B. Dynamic Load Frame Characterization

To achieve facility characterization, both acceleration at impact and the velocity of the falling plate are interrogated. The drop plate is instrumented with a PCB Piezotronics Model 356B20 piezoelectric triaxial accelerometer, which indicates the levelness of any given drop, translating to the squareness of the impact on the desired impact location. The drop tower is also instrumented with a photoelectric sensor which detects the interference geometry mounted to the drop plate, providing the timestamps at which the crossings occur. To improve the accuracy of each reading, there are three total crossings, each spaced 38 mm apart. The last two crossings for time measurement ($t_{2\to3}$) are used in the velocity estimation for kinetic energy at impact following Eq. (1).

$$v = \frac{0.0381m}{t_{2\to3}} \tag{1}$$

The kinetic energy at impact follows Eq. (2).

$$KE = \frac{1}{2}mv^2 \tag{2}$$

A characterization of the load frame in the context of the experiments presented is provided below in Table 1, with a drop height of 0.2794 m corresponding to a potential energy of 12.4 J.

Table 1 Impact test characterization data.

	Test 1	**Test 2**	**Test 3**	**Test 4**	**Test 5**	**Test 6**	**Test 7**	**Test 8**
$\Delta t_{1\to2}$ $\Delta t_{2\to3}$ **(ms)**	18.6 17.1	20.5 18.5	19.0 17.5	19.1 17.2	19.1 18.5	19.0 17.6	18.6 16.4	19.2 17.8
v (m/s)	2.23	2.06	2.18	2.22	2.06	2.16	2.32	2.14
KE (J)	11.3	9.6	10.8	11.2	9.6	10.7	12.3	10.4

C. Test Specimen Instrumentation

FBG sensors respond to strain when mechanical deformation alters the pitch between layers of a grating written into the optical fiber. Changes in this pitch induce a shift in the characteristic Bragg wavelength, λ_B. The Bragg wavelength serves as the baseline for strain measurement, and shifts from this baseline are then correlated to strain at a particular FBG, analogous to the way changes in resistance underscore RSG operation. Multiple gratings can be written along a single optical fiber, and the Bragg wavelengths of each grating can be multiplexed to deliver a data stream to a single channel. In this study, the FBGs are interrogated using a Wavelength Division Multiplexing (WDM) system designed by the Fiber Optic Strain Sensing (FOSS) Lab at NASA Armstrong Flight Research Center. The WDM system implements Sense 2020 software (BaySpec) to interrogate strain readings from the FBGs, which were sampled at 5 kHz.

The RSGs instrumented are 1000Ω SGD-10/1000-LY13 foil gauges (1) in a half-bridge configuration. The signal from the gauges was amplified using Futek IAA100 (2) signal amplifiers, with external Wheatstone bridge completion. The signal from the IAA100 is connected to a National Instruments DAQ board (USB-6221) and collected using NI LabVIEW, which samples at 2.5 kHz given the IAA100 bandwidth of 25 kHz.

The test specimen used in the study is a 140 mm internal diameter, 355.6 mm long, 10-ply carbon fiber rocket section. The section is instrumented with both an RSG and FBG collocated to measure the hoop strain 108 mm and 89 mm from the edge of the section, respectively. The sensors were applied using M-Bond GA-2 bonding adhesive (3). The point of impact was positioned at the intersection of the central longitudinal and central hoop axes of the test section, and the sensors were radially spaced 76.2 mm from the impact point. A detailed schematic of the test section instrumentation is provided below in Figure 2.

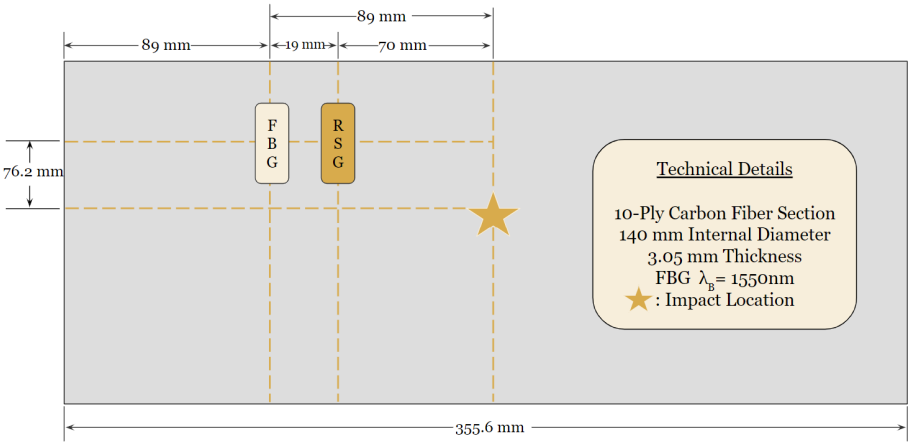

Fig. 2 Schematic of the test section instrumentation.

IV. Methods

Impact testing was completed under four distinct testing conditions as outlined below:

1) 6.35 mm thick CONFOR (4) foam padding underneath test specimen, no scoring done to the test section.
2) Rigid impact (no foam padding), no scoring done to the test section.
3) 6.35 mm thick CONFOR foam padding underneath test specimen, scoring done to the test section.
4) Rigid impact (no foam padding), scoring done to the test section.

All testing was conducted from a drop height of 27.94 cm, corresponding to a maximum equivalent energy of 12.4 J, as characterized in Table 1. Figure 3 shows the test section in the scored (artificially damaged) state.

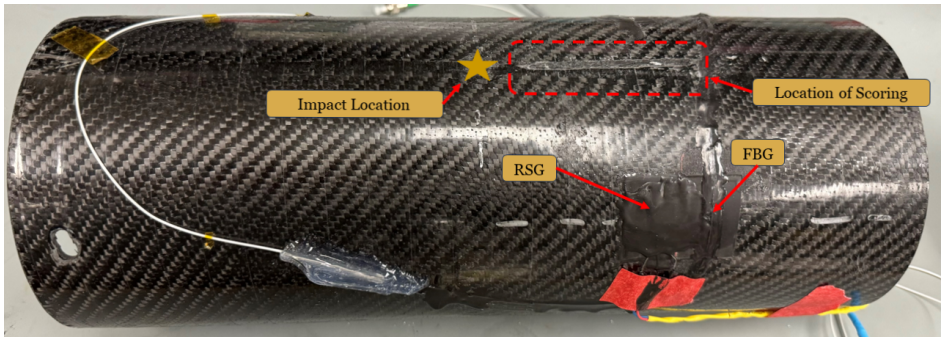

Fig. 3 Image of the scored test section.

V. Results

Across these studies, the RSG registers consistently larger peak strain values compared to the FBG given the proximity to impact (note Figure 2). Runs with the rigid impact condition (*no foam*) register higher overall peak strain values on account of the removal of any dampening. An overview of the collected strain data for each of the four runs is presented in Table 2. An in-depth discussion of each run is provided in subsequent sections.

Table 2 Tabulated strain data for Tests I - IV.

	KE (J)	FBG Microstrain ($\mu\varepsilon$)	RSG Microstrain ($\mu\varepsilon$)
Test I Foam Support, Undamaged	11.0	710	884
Test II Rigid Support, Undamaged	11.4	1424	1602
Test III Foam Support, Scored	12.0	1520	1661
Test IV Rigid Support, Scored	11.0	2102	2275

A. Test I

Figure 4 provides the resultant FBG and RSG strains in a time domain that synchronizes the strain signatures. This test validates the capability of both sensors to detect the complete duration and magnitude of the dynamic strain impact event. The results are further supported by the secondary and tertiary signals reported by both the FBG and RSG, as the drop plate rebounds on the impact surface. It is noted the rise-to-fall time of both sensor signals for Test I is approximately 15 ms.

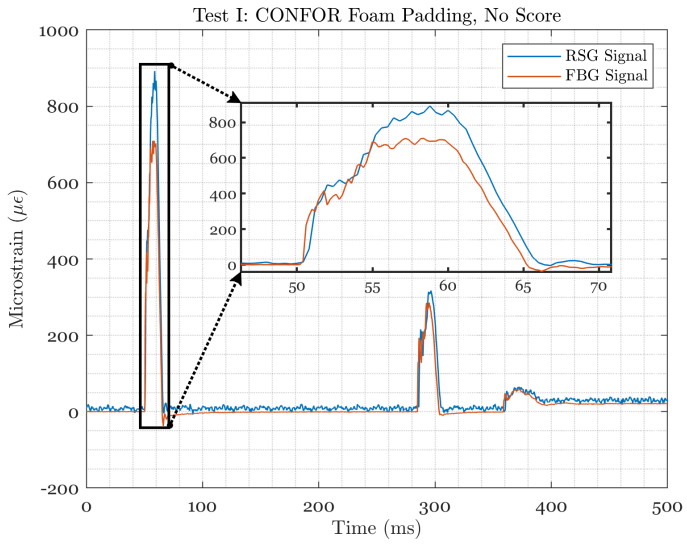

Fig. 4 Results from Test I, with CONFOR foam supporting the test section and no score on the surface.

B. Test II

Test II provides strong correlation results both in magnitude and time between sensors, which can be seen below in Figure 5. Of particular importance is the increase in the peak strain for the rigid impact condition compared to the foam-supported Test I. In addition, the time range of approximately 64 ms - 150 ms immediately following the initial signal spike shows a period of harmonic oscillation about the zero point due to the undamped condition of the test. It is noted in Test II the rise-to-fall times of both sensors are approximately 14 ms, aligning well with the results of Test I.

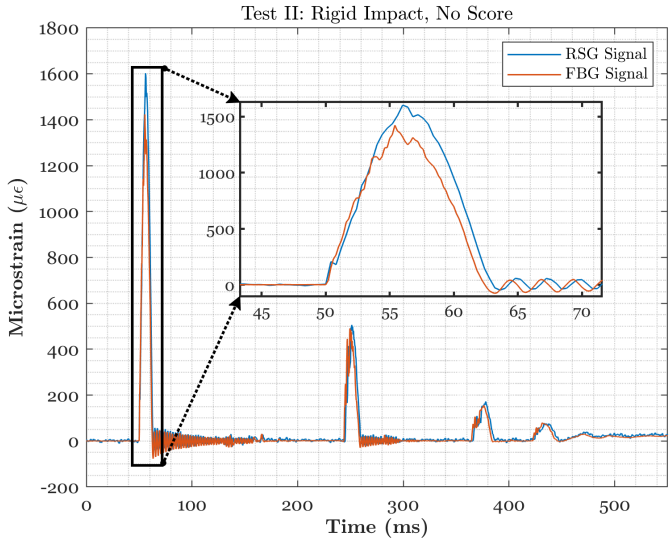

Fig. 5 Results from Test II, with rigid support and no score on the surface.

C. Test III

Test III results are provided in Figure 6 alongside the data from Test I. The strain data for the scored, foam-supported condition of Test III provided FBG and RSG peak strains of 1520 $\mu\varepsilon$ and 1661 $\mu\varepsilon$ respectively. This result supports the role of present specimen damage in increasing the resultant peak strain for a given impact when compared to Test I. The

individual sensor's rise-to-fall times are observed to be approximately 16 ms for Test III data.

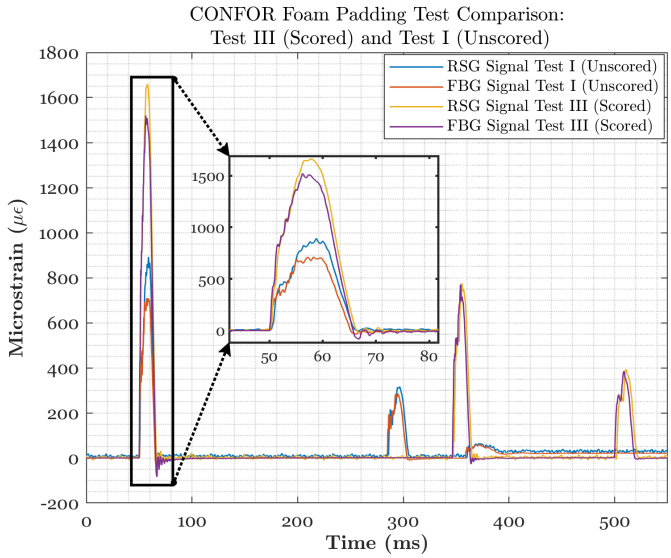

Fig. 6 Results from Test III, with CONFOR foam supporting the test section and a 76 mm long, 2.16 mm deep score into the 3.05 mm thick section.

D. Test IV

Results for Test IV are compared to Test II results and presented below in Figure 7. It is observed that the rise-to-fall times of the sensor peak signals is approximately 16 ms for Test IV data.

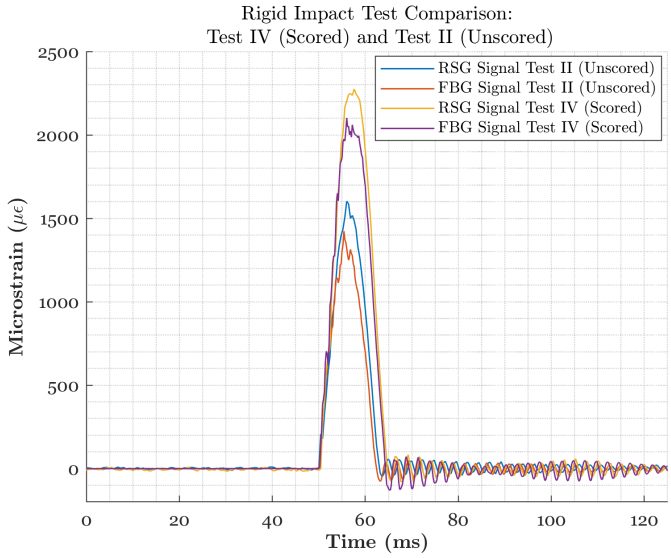

Fig. 7 Results from Test IV, with rigid support and a 76 mm long, 2.16 mm deep score into the 3.05 mm thick section.

VI. Conclusion

The results of the current study validate the capability of FBG sensors to interrogate dynamic strain events. It is observed that structural damage to a composite reusable airframe section significantly alters the measured dynamic strain for the same impact test conditions. Additionally, it is observed that sampling frequencies as low as 2.5 kHz are sufficient for detecting the dynamic strain events studied. FBG instrumentation has known benefits to RSG instrumentation and is easily adaptable to monitoring structural health in flight vehicles. In future work, the rise-to-fall times of the sensor signals will be the primary concern in the interrogation of blast events, as the blast timescale is shorter than that of the impact-based dynamic strain event timescale.

VII. Appendix

1) RSG Foil Gauges: (https://www.omega.com/en-us/force-and-strain-measurement/strain-gauges/linear-strain-gauges/sgd-linear1-axis/p/SGD-10-1000-LY13)
2) Futek IAA100: (https://www.futek.com/store/instruments/analog-amplifier/strain-gauge-analog-amplifier-voltage-output-IAA100/FSH03863)
3) M-Bond GA-2 Bonding Adhesive: (https://micro-measurements.com/pca/detail/mbond-ga2-kit)
4) CONFOR Foam: (https://www.cumulus-soaring.com/store/confor-foam)

VIII. Acknowledgements

The authors would like to thank the FOSS team and those adjacent at NASA AFRC who have trained us in the principles, application, use, and interrogation of fiber optic strain sensors and the WDM system. The authors would also like to thank Vanderbilt Aerospace Design Laboratory undergraduate independent study contributors for their role in helping to complete various phases of the research. The research conducted at VADL was supported by the Mark Dalton Fund for Experiential Learning in Aerospace Engineering.

References

[1] Barnoncel, D., Staszewski, W. J., Schell, J., and Peres, P., "Damage detection in reusable launch vehicle components using guided ultrasonic waves and 3D laser vibrometry," 2013. https://doi.org/10.1117/12.2009846.

[2] Frieden, J., Cugnoni, J., Botsis, J., and Gmür, T., "Low energy impact damage monitoring of composites using dynamic strain signals from FBG sensors - Part I: Impact detection and localization," *Composite Structures*, Vol. 94, 2012. https://doi.org/10.1016/j.compstruct.2011.08.003.

[3] Frieden, J., Cugnoni, J., Botsis, J., and Gmür, T., "Low energy impact damage monitoring of composites using dynamic strain signals from FBG sensors - Part II: Damage identification," *Composite Structures*, Vol. 94, 2012. https://doi.org/10.1016/j.compstruct.2011.08.025.

[4] Bouvier, C., and Emery, L., "Health management and non-destructive evaluation for reusable launch vehicles," 1994. https://doi.org/10.4271/942153.

[5] Friebele, E. J., Askins, C. G., Bosse, A. B., Kersey, A. D., Patrick, H. J., Pogue, W. R., Putnam, M. A., Simon, W. R., Tasker, F. A., Vincent, W. S., and Vohra, S. T., "Optical fiber sensors for spacecraft applications," *Smart Materials and Structures*, Vol. 8, 1999. https://doi.org/10.1088/0964-1726/8/6/310.

[6] Goossens, S., Geernaert, T., Khodaei, Z. S., Karachalios, E., Saenz-Castillo, D., and Berghmans, F., "Barely visible impact damage detection and location on composite materials by surface-mounted and embedded aerospace-compatible optical fibre Bragg grating sensors," 2020. https://doi.org/10.1117/12.2559262.

[7] Goossens, S., Berghmans, F., Khodaei, Z. S., Lambinet, F., Karachalios, E., Saenz-Castillo, D., and Geernaert, T., "Practicalities of BVID detection on aerospace-grade CFRP materials with optical fibre sensors," *Composite Structures*, Vol. 259, 2021. https://doi.org/10.1016/j.compstruct.2020.113243.

[8] Goossens, S., Muñoz, K., Jiménez, M., Karachalios, E., and Berghmans, F., "Global damage index of aerospace-grade CFRP subcomponents with FBG-based sensors," 2023. https://doi.org/10.1117/12.2678088.

[9] Panopoulou, A., Loutas, T., Roulias, D., Fransen, S., and Kostopoulos, V., "Dynamic fiber Bragg gratings based health monitoring system of composite aerospace structures," *Acta Astronautica*, Vol. 69, 2011. https://doi.org/10.1016/j.actaastro.2011.05.027.

[10] Alvarez-Montoya, J., Carvajal-Castrillón, A., and Sierra-Pérez, J., "In-flight and wireless damage detection in a UAV composite wing using fiber optic sensors and strain field pattern recognition," *Mechanical Systems and Signal Processing*, Vol. 136, 2020. https://doi.org/10.1016/j.ymssp.2019.106526.

[11] Mrad, N., "Potential of bragg grating sensors for aircraft health monitoring," *Transactions of the Canadian Society for Mechanical Engineering*, Vol. 31, 2007. https://doi.org/10.1139/tcsme-2007-0001.

[12] James, S. W., Tatam, R. P., Fuller, S. R., and Crompton, C., "Monitoring transient strains on a gun barrel using fibre Bragg-grating sensors," *Measurement Science and Technology*, Vol. 10, 1999. https://doi.org/10.1088/0957-0233/10/2/002.

[13] Ayers, J., Weerasooriya, T., Ghoshal, A., Pecora, C., Gunnarsson, A., Sanborn, B., and Turney, P., "Feasibility of component state awareness of high strain rate events using fiber Bragg grating sensors," *International Journal of Impact Engineering*, Vol. 100, 2017. https://doi.org/10.1016/j.ijimpeng.2016.10.012.

[14] Cusano, A., Cutolo, A., Nasser, J., Giordano, M., and Calabrò, A., "Dynamic strain measurements by fibre Bragg grating sensor," 2004. https://doi.org/10.1016/j.sna.2003.10.031.

[15] Li, H., Chen, W., and Hao, H., "Factors influencing impact force profile and measurement accuracy in drop weight impact tests," *International Journal of Impact Engineering*, Vol. 145, 2020. https://doi.org/10.1016/j.ijimpeng.2020.103688.

[16] O'Dwyer, M. J., Dykes, N. D., James, S. W., Tatam, R. P., and Irving, P. E., "Impact detection in carbon fiber reinforced polymer composites using in-fiber Bragg gratings," 1998. https://doi.org/10.1117/12.316449.